Progress In Electromagnetics Research M, Vol. 105, 21–30, 2021

A New Coupled-Line Based Dual-Band Branch-Line Coupler with Port-Extensions

Rakibul Islam[1], Asif I. Omi[2], Mohammad A. Maktoomi[3, *], Christine Zakzewski[3], and Praveen Sekhar[2]

Abstract—In this paper, a coupled-line based dual-band branch-line coupler with port-extensions is presented. The configuration of the coupler consists of a single coupled-lines section, two transmission lines, and an easy to analyze L-section impedance matching network at all four ports of the coupler. A detailed theoretical analysis is carried out to obtain the closed-form design equations to determine the design parameters of the coupling structure. It is observed that the proposed dual-band coupler can support wide band-ratio and arbitrary power division. To validate the proposed design concept, a prototype working at 0.9 GHz and 1.8 GHz is fabricated on a 60 mil Rogers 4003C substrate exhibiting excellent match between the simulated and measured results.

1. INTRODUCTION

Branch-line coupler (BLC) is one of the fundamental blocks in the field of microwave engineering [1]. Multi-band operation of a BLC enables its spectrum aggregation capability [2, 3] which is a primary technique to ensure real-time high-speed communication.

Conventional single band BLCs are implemented using quarter wavelength long branches resulting in spurious responses only at the odd harmonics of the fundamental frequency [1]. In contrast, multi-band designs are implemented by adding additional stubs [4] and half-wavelength sections [5] to the conventional structure, modifying the coupled-lines structures [6] or some other unique BLC structures [7, 8], by port-extension techniques [9–11], etc. Over the years, numerous works have been reported on different aspects of dual-band coupler performance, for example, bandwidth control [12] and enhancement [13], miniaturization [14], wider band-ratio support [15], arbitrary port impedance [11], and arbitrary power division [9–11, 16, 17].

For any dual-band coupler, two major design criteria are the band-ratio and arbitrary power division. All of the dual-band branch-line couplers mentioned in the literature either achieve a wide band-ratio [15] or support arbitrary power division [9–11, 16, 17]. In practice, a combination of both of these capabilities in a single structure would be useful in the design stage of a complex structure. Therefore, in this paper, a novel coupled-line based dual-band branch-line coupler is proposed to attain wider band-ratio range and arbitrary power division capability at the coupled and through port of the coupler.

This paper will begin with developing the design theory of the proposed coupler. Then, a prototype following the proposed circuit topography is fabricated and measured for comparison with the simulated response of the coupling structure. Finally, a comparison table of state-of-the-art port-extended BLCs is presented to demonstrate the novelty of the proposed structure.

Received 12 August 2021, Accepted 19 September 2021, Scheduled 30 September 2021
* Corresponding author: Mohammad A. Maktoomi (mohammad.maktoomi@scranton.edu).
[1] University of Illinois at Urbana-Champaign, USA. [2] Washington State University Vancouver, USA. [3] University of Scranton, Pennsylvania, USA.

2. DESIGN OF PROPOSED DUAL-BAND PORT EXTENDED COUPLED-LINES COUPLER

In Fig. 1, we have proposed a special type of branch-line coupler where the vertical transmission line sections of a conventional branch-line coupler are replaced by a single coupled-lines section having even and odd mode impedances Z_e and Z_o, respectively. The electrical length of the coupled transmission line is 2θ. Horizontal transmission line sections have a characteristic impedance of Z_t with the same electrical length of 2θ. The configuration has two axes of symmetry XX' and YY'. Based on these axes of symmetry, four different configurations of even-odd mode circuits are shown in Figs. 1(b)–(e). The variable Y denotes the characteristic admittance of the transmission line which is inversely related to the Z variables. Hence, $Y_e = 1/Z_e$, $Y_o = 1/Z_o$, $Y_t = 1/Z_t$. Equivalent admittances for each even-odd mode circuits can be derived as

$$Y_{ee} = j\left(Y_t \tan\theta + Y_e \tan\theta\right) = jY_1 \tag{1}$$

$$Y_{eo} = j\left(-Y_t \cot\theta + Y_o \tan\theta\right) = jY_4 \tag{2}$$

$$Y_{oe} = j\left(Y_t \tan\theta - Y_e \cot\theta\right) = jY_3 \tag{3}$$

$$Y_{oo} = j\left(-Y_t \cot\theta - Y_o \cot\theta\right) = jY_2 \tag{4}$$

Here, $j = \sqrt{-1}$. Equivalent admittances Y_{ee}, Y_{eo}, Y_{oe}, and Y_{oo} are complex quantities having imaginary values of Y_1, Y_4, Y_3, and Y_2, respectively.

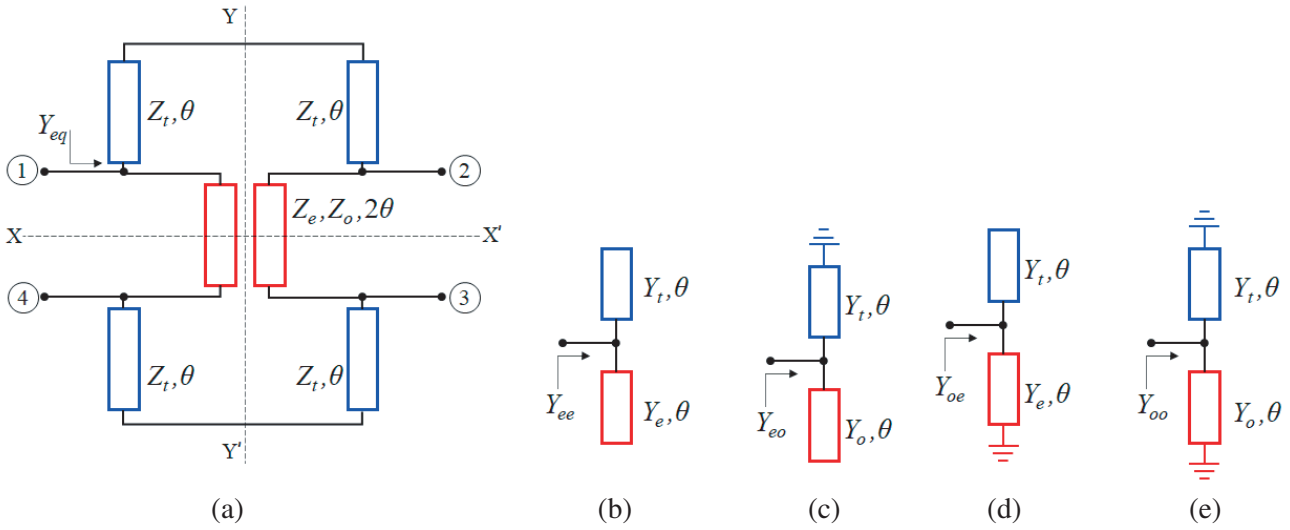

Figure 1. (a) Core of the coupled-lines based dual-band branch-line coupler and equivalent circuit configurations of the proposed coupler under the even- and odd-mode excitation: (b) even-even, (c) even-odd, (d) odd-even, (e) odd-odd.

According to [18], the equivalent input admittance looking at any port of the coupler of Fig. 1(a) is denoted by $Y_{eq} = G_{eq} + jB_{eq}$. Here, G_{eq} and B_{eq} are the equivalent input conductance and susceptance of the coupler, respectively. Their expressions can be derived as

$$B_{eq} = \frac{Y_2Y_3 - Y_1Y_4}{Y_2 + Y_3 - Y_1 - Y_4} \tag{5}$$

$$G_{eq} = \sqrt{B_{eq}\left(Y_1 + Y_4\right) - Y_1Y_4 - B_{eq}^2} \tag{6}$$

Once the value of Y_{eq} is calculated using Eqs. (5) and (6), dual-band port-extended impedance matching networks can be implemented to realize a functioning dual-band coupler. It follows from Eq. (6) that to make G_{eq} a positive real value, the following inequality must be met

$$\left(B_{eq} - Y_1\right)\left(B_{eq} - Y_4\right) < 0 \tag{7}$$

In a dual-band design, the electrical length and design frequencies are interdependent [9]. If the two design frequencies are f_1 and f_2, where $f_2 > f_1$ and the dual-band frequency-ratio is $r = f_2/f_1$, then for a dual-band operation, the electrical length θ at f_1 can be obtained as

$$\theta|_{f_1} = \frac{m\pi}{1+r} \tag{8}$$

Equation (9) gives the value of θ at f_2 as

$$\theta|_{f_2} = m\pi - \theta|_{f_1} \tag{9}$$

Here m can be any integer value. The relation of θ at f_1 and f_2 given in Eq. (9) dictates the complex conjugate relationship in Eqs. (1)–(6). In other words,

$$Y_{eq}|_{f_1} = {Y_{eq}}^*|_{f_2} \Rightarrow G_{eq}|_{f_1} + j\,B_{eq}|_{f_1} = G_{eq}|_{f_2} - j\,B_{eq}|_{f_2} \tag{10}$$

Equations (6) and (5) are plotted in Fig. 2(a) and Fig. 2(b), respectively. Both the plots validate Eq. (10) by showing that for a fixed set of Z_e, Z_o, and Z_t, G_{eq} has an even symmetry whereas B_{eq} has an odd symmetry with respect to the same asymptote at $\theta = 90°$. The ratio of S_{21} and S_{31} of the coupler is related to the power division parameter k, $(k > 0)$ as below

$$S_{21} = jkS_{31} \tag{11}$$

Here, $20\log(k)$ denotes the power division ratio in dB. The definitions of S_{21} and S_{31} for a symmetrical four-port network reduce to the following [10]

$$S_{21} = \frac{1}{2}\left(\Gamma_{ee} - \Gamma_{oo}\right) \tag{12}$$

$$S_{31} = \frac{1}{2}\left(\Gamma_{ee} + \Gamma_{oo}\right) \tag{13}$$

Here, the reflection coefficients for the even-even (Γ_{ee}) and odd-odd (Γ_{oo}) cases are given by

$$\Gamma_{ee} = \frac{Y_{eq} - Y_{ee}}{{Y_{eq}}^* + Y_{ee}}\left(\frac{{Y_{eq}}^*}{Y_{eq}}\right) = \frac{|Y_{eq}|^2 - Y_{ee}{Y_{eq}}^*}{|Y_{eq}|^2 + Y_{ee}Y_{eq}} \tag{14}$$

$$\Gamma_{oo} = \frac{Y_{eq} - Y_{oo}}{{Y_{eq}}^* + Y_{oo}}\left(\frac{{Y_{eq}}^*}{Y_{eq}}\right) = \frac{|Y_{eq}|^2 - Y_{oo}{Y_{eq}}^*}{|Y_{eq}|^2 + Y_{oo}Y_{eq}} \tag{15}$$

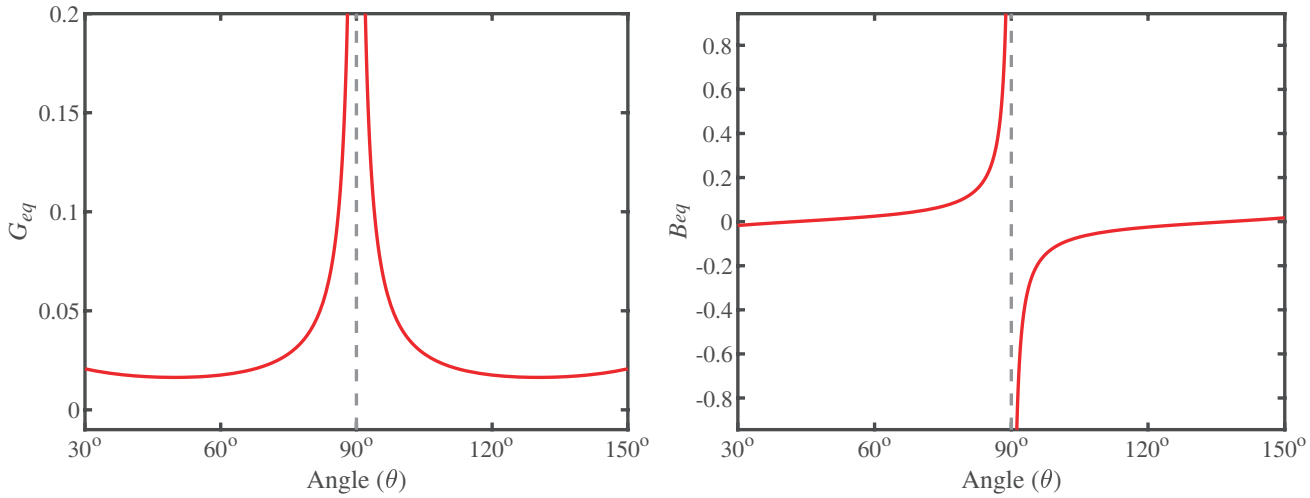

Figure 2. Plot of (a) G_{eq} and (b) B_{eq} versus θ for $Z_e = 80\,\Omega$, $Z_o = 60\,\Omega$, and $Z_t = 45\,\Omega$, according to Eqs. (6) and (5), respectively.

Now using Eqs. (12) and (13) in Eq. (11), the power division ratio can be derived as

$$\frac{S_{21}}{S_{31}} = \frac{\Gamma_{ee} - \Gamma_{oo}}{\Gamma_{ee} + \Gamma_{oo}} = jk \tag{16}$$

Using Eqs. (14) and (15) into Eq. (16) yields:

$$\frac{G_{eq}\left(Y_2 - Y_1\right)}{\left(G_{eq}^2 + B_{eq}^2\right) - B_{eq}\left(Y_2 + Y_1\right) + Y_2 Y_1} = k \tag{17}$$

$$G_{eq}\left(Y_2 - Y_1\right) - kG_{eq}^2 = k\left(B_{eq} - Y_1\right)\left(B_{eq} - Y_2\right) \tag{18}$$

For any value of k, both sides of Eq. (18) must be equal which requires the computation of Eqs. (1)–(6). According to Eq. (8), once the frequency ratio r is selected, the electrical lengths of all the transmission lines are known. The only variables to be considered are Z_e, Z_o, and Z_t. The choices of Z_e and Z_o values are limited by the realizable width and separation of the coupled-lines, whereas Z_t can take any values from 20 Ω–120 Ω depending on the microstrip line technology. The process of calculating the values of these three variables is described in the flow chart of Fig. 3. Using the flowchart with an appropriate value of Z_e, Z_o pair and known values of k and r, the value of Z_t can be calculated so that the obtained solutions always satisfy Eq. (18). For $k = 0$ dB (equal-power division case), Fig. 4(a) shows the plot of Z_t with respect to r, and it ranges from 47 Ω to 67 Ω for different values of (Z_e, Z_o) pairs. Fig. 4(b) plots calculated G_{eq} and B_{eq} using Eqs. (6) and (5) for different (Z_e, Z_o) pairs with respect to frequency ratio r. It is apparent from Fig. 4(b) that as the value of r increases, G_{eq} decreases and converges to a lower value whereas B_{eq} at first decreases, reaches a minimum, and then increases. This indefinite increase of B_{eq} limits the use of port impedance matching network (IMN) at each input port of the core of the coupler shown in Fig. 1. The purpose of IMN is to match the resulting Y_{eq} from Eqs. (5) and (6) to port termination impedance, Z_p (normally equal to $Z_0 = 50\,\Omega$). From the plot of Fig. 4(b), it is evident that the IMN must be capable of transforming this wide range of Y_{eq} to port termination impedance, Z_p. As r increases, different IMN configurations need to be considered to match the ports to the core of the coupler. In this paper, a simple L-section matching network is employed, shown in Fig. 5, to match the complex valued admittance, Y_{eq}, to real valued port termination impedance, Z_p. The (Z_1, θ_1) line transfers Y_{eq} to Y_{ex} using Eq. (19) where Z_{ex} is given in Eq. (20).

$$Y_{ex} = G_{ex} + jB_{ex} = \frac{1}{Z_{ex}} \tag{19}$$

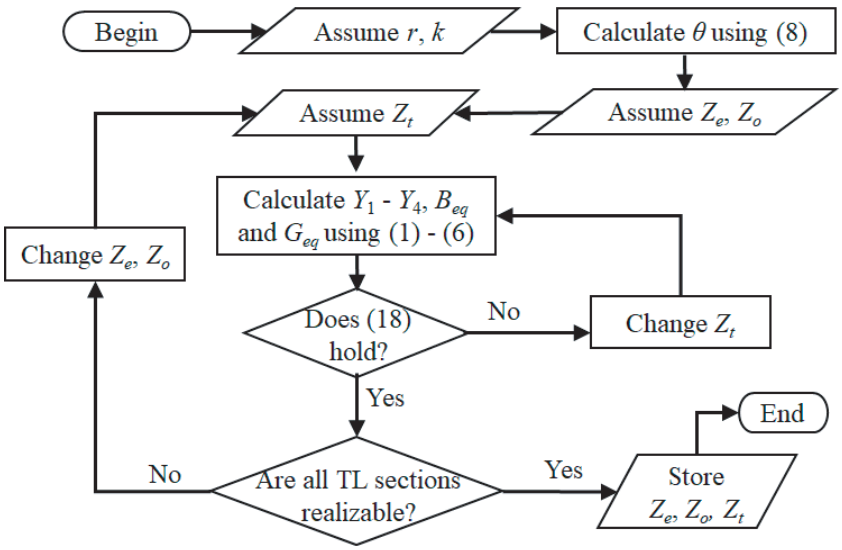

Figure 3. Flow chart for designing the core of the coupler.

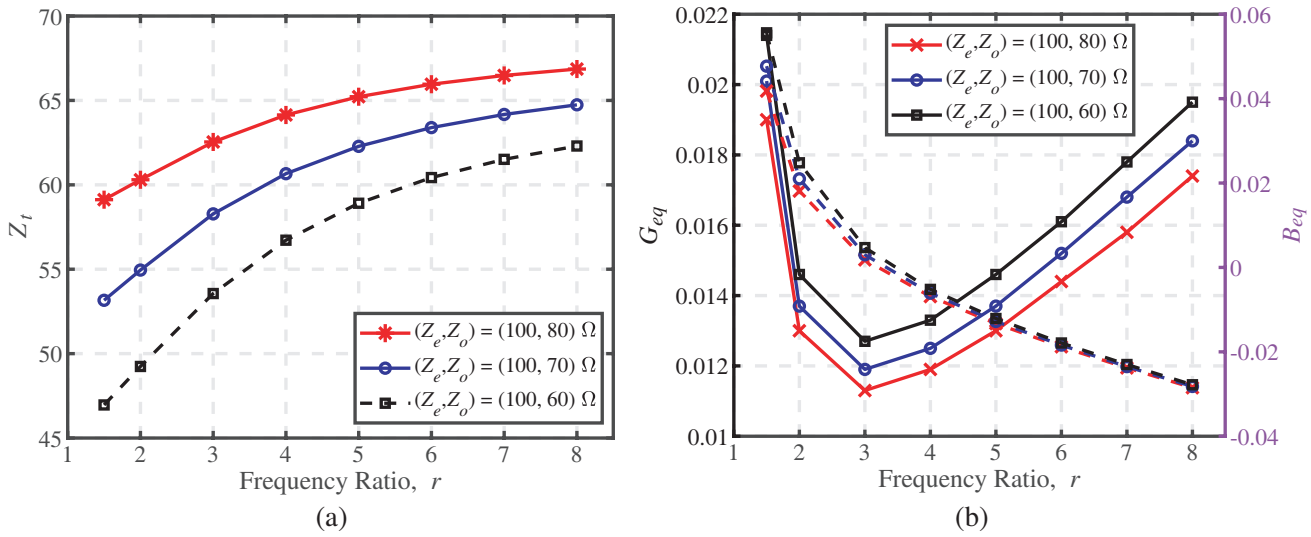

Figure 4. (a) Calculated values of Z_t supporting (18) for different Z_e, Z_o pairs. (b) Calculated values of real and imaginary parts of core admittance Y_{eq} using the values of Z_t obtained in Fig. 4(a). These plots are for $k = 0\,\text{dB}$.

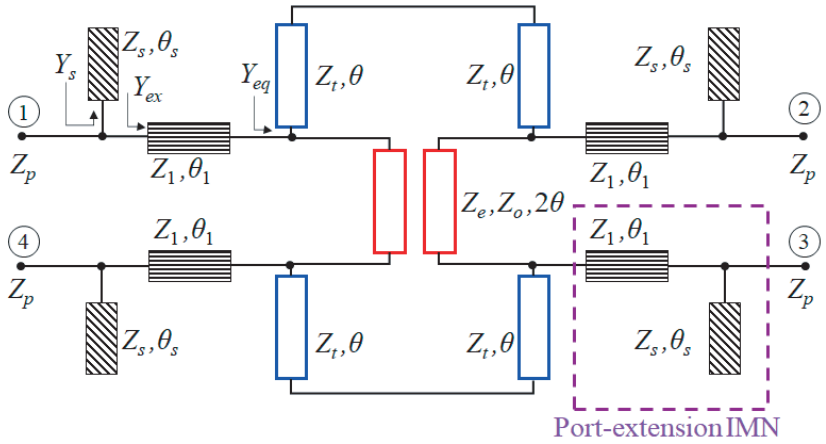

Figure 5. Proposed port-extended dual-band coupler.

$$Z_{ex} = Z_1 \frac{R_{eq} + j\left(X_{eq} + Z_1 a\right)}{\left(Z_1 - X_{eq} a\right) + j R_{eq} a} \tag{20}$$

$$G_{ex} = \frac{R_{eq}\left(1 + a^2\right)}{R_{eq}^2 + \left(X_{eq} + Z_1 a\right)^2} \tag{21}$$

Here, $a = \tan(\theta_1)$. For dual-band operation, the value of θ_1 is determined using Eq. (22) which is similar to Eq. (8), and p can be any positive integer. The purpose of the characteristic impedance Z_1 is to transfer Y_{eq} to Y_{ex} so that its real part G_{ex} given in Eq. (21) becomes equal to port termination admittance, Y_p $(= 1/Z_p)$. This leads to a quadratic equation in Z_1 as given in Eq. (23).

$$\theta_1|_{f_1} = \frac{p\pi}{1 + r} \tag{22}$$

$$a^2 Z_1^2 + 2 X_{eq} a Z_1 + \left[R_{eq}^2 + X_{eq}^2 - Z_p R_{eq}\left(1 + a^2\right)\right] = 0 \tag{23}$$

A realizable solution of Z_1 from Eq. (23) will equalize G_{ex} to the port admittance Y_p. The remaining susceptance can be calculated using Eq. (24). The stub admittance Y_s should be able to cancel

this remaining B_{ex}. This capability depicts the performance of IMN in transforming Y_{eq} to Z_p. To incorporate design flexibility, the stub can either be short or open-circuited with characteristic impedance Z_s. For dual-band operation, the value of θ_s is limited by Eq. (25) where q can be any integer value. The characteristic impedance Z_s is calculated using Eq. (26) from the values obtained in Eqs. (24) and (25).

$$B_{ex} = \frac{R_{eq}^2 a - (Z_1 - X_{eq}a)(X_{eq} + Z_1 a)}{Z_1\left[R_{eq}^2 + (X_{eq} + Z_1 a)^2\right]} \tag{24}$$

$$\theta_s|_{f_1} = \frac{q\pi}{1+r} \tag{25}$$

$$Z_s = \begin{cases} -\tan(\theta_s)/B_{ex}; & \text{open stub} \\ \cot(\theta_s)/B_{ex}; & \text{shorted stub} \end{cases} \tag{26}$$

A summary for the design flow is shown in the flowchart of Fig. 6(a). A combination of flowcharts shown in Fig. 3 and Fig. 6(a) is used to obtain a set of design parameters, namely, (Z_e, Z_o) pair, Z_t, Z_1, and Z_s for different r and k values for the novel port-extended coupling structure shown in Fig. 5. The novelty of the structure is two-fold. It supports an extremely wide range of both frequency ratio, r, and power division ratio, k. To show this wide supporting range, a set of plots and tables are generated. At first, the value of k is fixed at 0 dB, and the calculated design parameters are plotted in Fig. 6(b) with respect to dual-band frequency ratio, r. It is evident from the plot that for $k = 0$ dB, the port-extended branch-line coupler supports the dual-band ratio of 1.5–8.

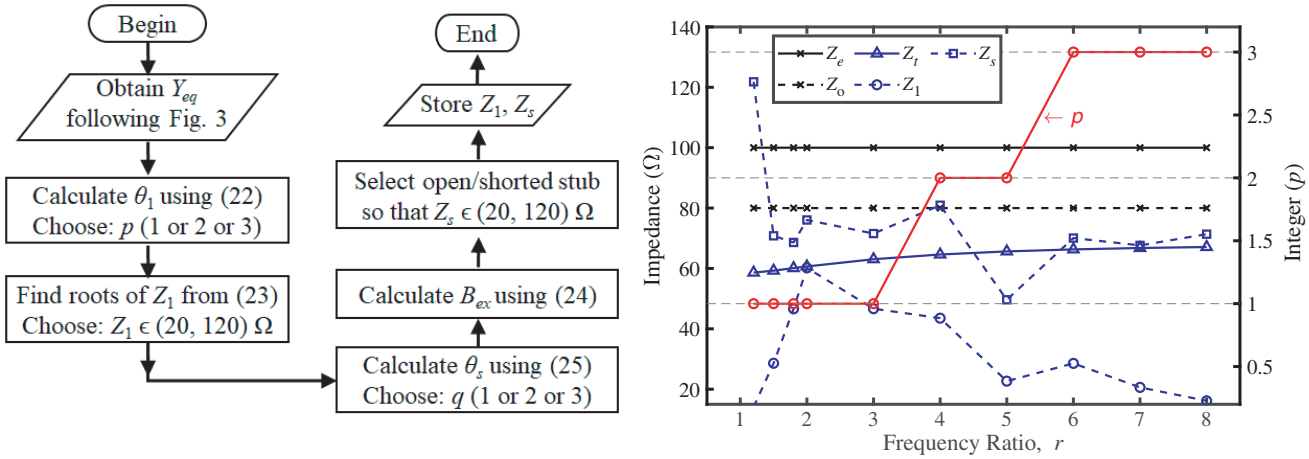

Figure 6. (a) Flow chart for calculating design parameters for the configuration shown in Fig. 5. (b) Plot of required characteristic impedances (Z_t, Z_1, and Z_s), (Z_e, Z_o) pair, for different electrical lengths defined by (8), (22), and (25) respectively. The value of m and q are kept at 1 whereas p varies from 1 to 3 to reduce the overall size of the structure for $k = 0$ dB.

Table 1 displays the calculated design parameters for extreme band-ratio cases. It dictates the capability of the proposed coupling structure in supporting high r and k values. For example, the first row of the table is for $r = 1.5$ where all the design parameters are in practical range for different k values, namely, 2 dB, 8 dB, and 11.76 dB. It is also clear that, for $k = 2$ dB, the proposed coupler supports the r value of 1.5–7. For $k = 8$ dB, the r value ranges from 1.5 to 11 whereas for $k = 11.76$ dB, the r value ranges from 1.5–12.

3. SIMULATION AND MEASUREMENT RESULTS

To validate the proposed design concept for the port-extended branch-line coupler, a prototype has been designed, simulated, and fabricated using the proposed design configuration. A dual-band port-

Table 1. Calculated design parameters m, (Z_e, Z_o) pair, Z_t, p, Z_1, q, and Z_s for different r values at $k = 2\,\text{dB}$, $8\,\text{dB}$, and $11.76\,\text{dB}$.

r	k [dB]	m	(Z_e, Z_o) [Ω]	Z_t [Ω]	p	Z_1 [Ω]	Stub type	q	Z_s [Ω]
1.5	2	1	(100,80)	52.55	1	27.94	Open	1	77.44
	8	1	(100,80)	31.99	1	23.41	Open	1	87.71
	11.76	1	(100,80)	21.97	1	19.80	Open	1	86.28
3	2	1	(100,90)	58.97	1	48.30	Short	1	108.78
	8	1	(100,80)	33.05	1	52.05	Open	1	127.29
	11.76	1	(100,80)	22.35	1	44.69	Open	1	69.98
7	2	1	(100,80)	58.36	3	22.24	Short	1	92.71
	8	1	(100,80)	34.05	3	22.70	Short	2	109.01
	11.76	1	(100,80)	22.80	2	22.16	Open	1	28.58
11	8	1	(100,80)	34.28	2	21.80	Open	2	20.40
	11.76	1	(100,80)	22.91	2	22.66	Open	3	25.72
12	11.76	1	(100,80)	22.92	2	23.33	Open	3	20.25

extended branch-line coupler prototype working at 0.9 GHz and 1.8 GHz ($r = 2$) with equal-power division ($k = 0\,\text{dB}$) at the through (port 2) and coupled port (port 3) of the coupler is fabricated on a Rogers 4003C board. The substrate has a dielectric constant of 3.55, thickness of 1.575 mm, loss tangent of 0.0022, and copper cladding of 35 μm on both sides. It is found that unity value of m, p, and q in Eqs. (8), (22), and (25) in the proposed circuit configuration of Fig. 5 can support the dual-band operation for $r = 2$. This leads to the electrical length for all the transmission lines (θ, θ_1, and θ_s) equal to 60°.

The circuit parameters are calculated for a port impedance, $Z_p = 50\,\Omega$ using the flowchart of Fig. 3 and Fig. 6(a) as: $Z_e = 100\,\Omega$, $Z_o = 80\,\Omega$, $Z_t = 60.66\,\Omega$, $Z_1 = 60.19\,\Omega$, and $Z_s = 76.05\,\Omega$ at the first design frequency $f_1 = 0.9\,\text{GHz}$. The photo of the fabricated prototype is shown in Fig. 7(a). The physical dimensions are shown in mils (thousandth of an inch). The scattering parameters of the designed prototype are measured using a Tektronix TT506A Vector-Network Analyzer (VNA). The measurement setup is shown in Fig. 7(b) where the VNA display on the computer screen shows the measured $|S_{21}|$. The EM simulated results obtained using the Keysight ADS vs the measured S-parameter magnitude response are shown in Fig. 8(a). It is apparent from the plots that the measured

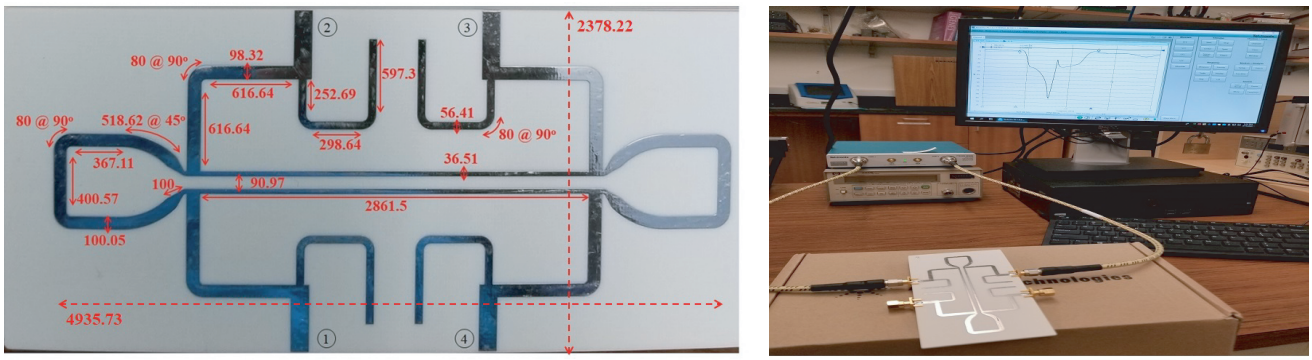

Figure 7. (a) Fabricated prototype of the dual-band port-extended branch-line coupler. All dimensions are in mils. (b) Test setup for the measurement of the S-parameters for the fabricated prototype shown in Fig. 7(a).

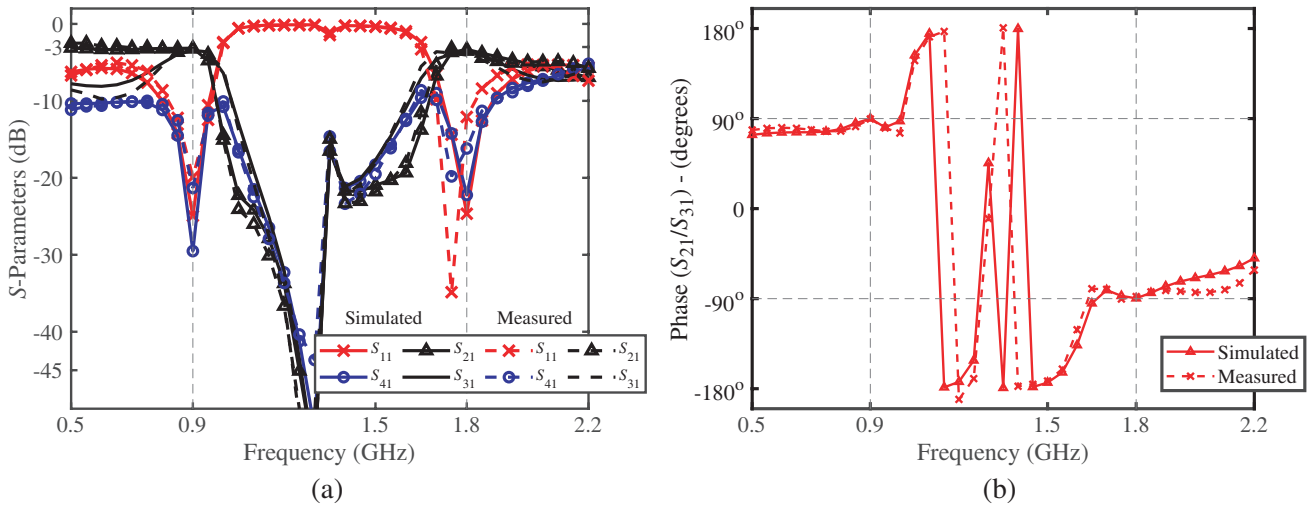

Figure 8. Simulated vs. measured results — (a) S-parameter magnitude response of the dual-band coupler; (b) Phase difference between the through and coupled port of the coupler.

and simulated data correlate well with each other having return loss and isolation loss better than 20 dB at both design frequencies. For a 10 dB reference, the return loss bandwidths are 143 MHz @f_1 / 118 MHz @f_2, and the isolation loss bandwidths are 150 MHz @f_1 / 180 MHz @f_2. The transmission bandwidths in this region are 120 MHz @f_1 / 100 MHz @f_2. Although the overall magnitude responses of S_{11} and S_{41} shift slightly from the intended second center frequency of 1.8 GHz due to fabrication tolerances, the 10 dB bandwidth still supports the proposed/simulated regions of operation. If desired,

Table 2. Comparison table between the proposed and state-of-the-art port-extended couplers. Here, λ_o is the free space wavelength.

Ref.	Power Division Capability	$20\log(k)$ [dB]	Band-Ratio Range, r	Port Terminations, Z_p	Fabricated Device Sizes, $W \times L$
[10]	Equal	0	1–3	Equal	$0.35\lambda_o \times 0.17\lambda_o$ [λ_o @1 GHz, $r = 2$, $k = 0$ dB]
[11]	Arbitrary	11.76	1–1.93	Arbitrary	$0.85\lambda_o \times 0.23\lambda_o$ [λ_o @1.25 GHz, $r = 1.5$, $k = 0$ dB]
[9]	Arbitrary	0 2 8 11.76	1.4–3.35 1.55–3.4 1.55–2.95 1.65–3	Arbitrary	$0.32\lambda_o \times 0.15\lambda_o$ [λ_o @1.2 GHz, $r = 2.1$, $k = 6$ dB] $0.32\lambda_o \times 0.19\lambda_o$ [λ_o @1 GHz, $r = 2$, $k = 2$ dB]
This Work	Arbitrary	0 2 8 11.76	1.5–8 1.5–7 1.5–11 1.5–12	Arbitrary	$0.38\lambda_o \times 0.18\lambda_o$ [λ_o @0.9 GHz, $r = 2$, $k = 0$ dB]

this shift can be fixed with post-fabrication tuning coupled with simulation. In Fig. 8(b), the simulated and measured phase differences between port 2 and port 3 of the coupler are plotted. The measured result is in correlation with the simulated results at both the design frequencies. The measured phase differences are found to be 89.60° @f_1/ -90.10° @f_2.

A comparison table between the proposed coupler and the state of the art port-extended couplers is presented in Table 2. It is shown in the table that the proposed coupling structure supports wide range of band-ratios of 1.5–8 at $k = 0\,\text{dB}$, 1.5–7 at $k = 2\,\text{dB}$, 1.5–11 at $k = 8\,\text{dB}$, and 1.5–12 at $k = 11.76\,\text{dB}$. The fabricated device size is comparable to the state-of-the-art port-extended branch line couplers. Therefore, in the design of microstrip line based planar port-extended coupling structures, the proposed design configuration can support extensively large band ratio at arbitrary power division values.

4. CONCLUSION

In this paper, a novel port-extended dual-band branch-line coupler has been designed for the first time which supports extensively high band-ratio and arbitrary power division. The closed-form analytical design equations are derived, and a simple flow chart is presented to obtain the set of design parameters for arbitrary band-ratio and power division values. To prove the design concept, a prototype has been designed, fabricated, and measured. The measured and simulated results match quite well supporting the design theory of the proposed coupler.

ACKNOWLEDGMENT

Mohammad Maktoomi and Christine Zakzewski would like to acknowledge the support from the Dean of the College of Arts and Sciences, Dr. Michelle Maldonado, the Department of Physics and Engineering chairperson, Dr. W. Andrew Berger; Cadence for their AWRDE tool; and Rogers Corp. for the laminate samples.

REFERENCES

1. Pozar, D. M., *Microwave Engineering* , John Wiley & Sons, 2011.
2. Islam, R., M. H. Maktoomi, Y. Gu, and B. Arigong, "Concurrent dual-band microstrip line Hilbert transformer for spectrum aggregation real-time analog signal processing," *IEEE MTT-S Int. Microw. Symp. Dig.*, 900–903, Los Angeles, CA, USA, Aug. 2020.
3. Islam, R., M. H. Maktoomi, H. Ren, and B. Arigong, "Spectrum aggregation dual-band and real-time RF/microwave analog signal processing from microstrip line high-frequency Hilbert transformer," *IEEE Trans. Microw. Theory Techn.*, Vol. 1, No. 1, 1–1, 2021.
4. Cheng, K. M. and F. L. Wong, "A novel approach to the design and implementation of dual-band compact planar 90 branch-line coupler," *IEEE Trans. Microw. Theory Techn.*, Vol. 52, No. 11, 2458–2462, 2004.
5. Wong, F. L. and K. M. Cheng, "A novel planar branch-line coupler design for dual-band applications," *IEEE MTT-S Int. Dig.*, 903–906, Jun. 2004.
6. Zaidi, A. M., S. A. Imam, B. Kanaujia, and K. Rambabu, "A new equal power quadrature branch-line coupler for dual-band applications," *Progress In Electromagnetics Research Letters*, Vol. 74, 61–67, 2018.
7. Park, M. J. and B. Lee, "Dual-band, cross coupled branch-line coupler," *IEEE Microw. Wireless Compon. Lett.*, Vol. 15, No. 10, 655–657, 2005.
8. Cao, Y., J. Wen, H. Hong, and J. Liu, "Design of planar dual-band branch-line coupler with π-shaped coupled-lines," *Progress In Electromagnetics Research Letters*, Vol. 55, 113–120, 2015.
9. Maktoomi, M. A., M. S. Hashmi, and F. M. Ghannouchi, "A dual-band port-extended branch-line coupler and mitigation of the band-ratio and power division limitations," *IEEE Trans. Compon. Packag. Manuf. Techn.*, Vol. 7, No. 8, 1313–1323, 2017.

10. Kim, H., B. Lee, and M. Park, "Dual-band branch-line coupler with port extensions," *IEEE Trans. Microw. Theory Techn.*, Vol. 58, No. 3, 651–655, 2010.
11. Wu, Y., S. Y. Zheng, S. W. Leung, Y. Liu, and Q. Xue, "An analytical design method for a novel dual-band unequal coupler with four arbitrary terminated resistances," *IEEE Trans. Ind. Electron.*, Vol. 61, No. 10, 5509–5516, Oct. 2014.
12. Cheng, K. M. and S. Yeung, "A novel dual-band 3-dB branch-line coupler design with controllable bandwidths," *IEEE Trans. Microw. Theory Techn.*, Vol. 60, No. 10, 3055–3061, 2012.
13. Collado, C., A. Grau, and F. D. Flaviis, "Dual-band planar quadrature hybrid with enhanced bandwidth response," *IEEE Trans. Microw. Theory Techn.*, Vol. 54, No. 1, 180–188, 2006.
14. Jung, S. C., R. Negra, and F. M. Ghannouchi, "A design methodology for miniaturized 3-db branch-line hybrid couplers using distributed capacitors printed in the inner area," *IEEE Trans. Microw. Theory Techn.*, Vol. 56, No. 12, 2950–2953, 2008.
15. Zaidi, A. M., M. T. Beg, B. K. Kanaujia, K. Srivastava, and K. Rambabu, "A dual band branch-line coupler with wide frequency ratio," *IEEE Access*, Vol. 7, 25046–25052, 2019.
16. Wang, X., W. Yin, and K. Wu, "A dual-band coupled-line coupler with an arbitrary coupling coefficient," *IEEE Trans. Microw. Theory Techn.*, Vol. 60, No. 4, 945–951, 2012.
17. Zheng, S. Y., Y. Wu, Y. Li, Y. Liu, and Y. Long, "Dual-band hybrid coupler with arbitrary power division ratios over the two bands," *IEEE Trans. Compon. Packag. Manuf. Techn.*, Vol. 4, No. 8, 1347–1358, 2014.
18. Riblet, G. P., "A directional coupler with very flat coupling," *IEEE Trans. Microw. Theory Techn.*, Vol. 26, No. 2, 70–74, 1978.